

# UC Davis

## UC Davis Previously Published Works

### Title

Plasma-derived extracellular vesicles (EVs) as biomarkers of sepsis in burn patients via label-free Raman spectroscopy

### Permalink

<https://escholarship.org/uc/item/88p4j2cm>

### Journal

Journal of Extracellular Vesicles, 13(9)

### ISSN

2001-3078

### Authors

O'Toole, Hannah J

Lowe, Neona M

Arun, Vishalakshi

et al.

### Publication Date

2024-09-01

### DOI

10.1002/jev2.12506

Peer reviewed

# Plasma-derived extracellular vesicles (EVs) as biomarkers of sepsis in burn patients via label-free Raman spectroscopy

Hannah J. O'Toole<sup>1</sup>  | Neona M. Lowe<sup>1</sup>  | Vishalakshi Arun<sup>2</sup> | Anna V. Kolesov<sup>1</sup>  | Tina L. Palmieri<sup>3,4</sup>  | Nam K. Tran<sup>5</sup>  | Randy P. Carney<sup>1</sup> 

<sup>1</sup>Department of Biomedical Engineering, University of California, Davis, California, USA

<sup>2</sup>Department of Neurobiology, Physiology, and Behavior, University of California, Davis, California, USA

<sup>3</sup>Division of Burn Surgery, University of California, Davis Health, Firefighters Burn Institute Regional Burn Center, Sacramento, California, USA

<sup>4</sup>Shriners Children's Northern California, Sacramento, California, USA

<sup>5</sup>Department of Pathology and Laboratory Medicine, University of California, Davis, Sacramento, California, USA

## Correspondence

Randy P. Carney, Department of Biomedical Engineering, University of California, 1 Shields Ave., Davis, CA 95616, USA.  
Email: rcarney@ucdavis.edu

## Funding information

NIH/NCI, Grant/Award Numbers: R01 CA241666, T32GM136597, T32HL007013, R00GM080249

## Abstract

Sepsis following burn trauma is a global complication with high mortality, with ~60% of burn patient deaths resulting from infectious complications. Diagnosing sepsis is complicated by confounding clinical manifestations of the burn injury, and current biomarkers lack the sensitivity and specificity required for prompt treatment. There is a strong rationale to assess circulating extracellular vesicles (EVs) from patient liquid biopsy as sepsis biomarkers due to their release by pathogens from bacterial biofilms and roles in the subsequent immune response. This study applies Raman spectroscopy to patient plasma-derived EVs for rapid, sensitive, and specific detection of sepsis in burn patients, achieving 97.5% sensitivity and 90.0% specificity. Furthermore, spectral differences between septic and non-septic burn patient EVs could be traced to specific glycoconjugates of bacterial strains associated with sepsis morbidity. This work illustrates the potential application of EVs as biomarkers in clinical burn trauma care and establishes Raman analysis as a fast, label-free method to specifically identify features of bacterial EVs relevant to infection amongst the host background.

## KEYWORDS

bacterial EVs (bEVs), diagnostics, exosomes, systemic inflammatory response syndrome (SIRS)

## 1 | INTRODUCTION

Sepsis is characterized as a dysregulated systemic response to infection causing life-threatening organ dysfunction and devastating consequences if not promptly recognized and treated (Singer et al., 2016). Sepsis is a global health crisis accounting for an estimated 19.7% of all global deaths in 2017 (Rudd et al., 2020). Clinical indications of sepsis include an increase in the sequential (sepsis-related) organ failure assessment (SOFA) score by two points (or about 10% greater chance of in-hospital morbidity). A quick SOFA (qSOFA) may be performed to rapidly identify patients at risk of sepsis and subsequent septic shock (qSOFA, Shahsavarinia et al., 2020). This includes presenting with at least two of the following: systolic blood pressure 100 mmHg, respiratory rate 22 breaths/min, or altered mental status (Singer et al., 2016). Due to the morbidity of organ dysfunction, any patient who presents with infection should be monitored for sepsis. However, due to the heterogeneity of patient and pathogen factors, sepsis can present differently from patient to patient, making it difficult to definitively diagnose.

The clinical phenotype of sepsis becomes further altered when the patient sustains injury due to a temperature-related event, for example, a burn patient. Burn patients have a higher susceptibility to bacterial invasion and sepsis due to the compromised

This is an open access article under the terms of the [Creative Commons Attribution-NonCommercial-NoDerivs License](https://creativecommons.org/licenses/by-nc-nd/4.0/), which permits use and distribution in any medium, provided the original work is properly cited, the use is non-commercial and no modifications or adaptations are made.

© 2024 The Author(s). *Journal of Extracellular Vesicles* published by Wiley Periodicals LLC on behalf of International Society for Extracellular Vesicles.

skin barrier and already present systemic dysregulation and immunosuppression in response to burn trauma (Church et al., 2006). Burn wound infection is a major cause of burn patient death after the first 24 h post-trauma and resuscitation (Boehm & Menke, 2021). The diagnosis of sepsis in burn patients is complicated due to confounding clinical manifestations of the burn itself, negating the use of qSOFA and many other traditional criteria for sepsis. Prognosis for septic burn patients is poor, with recent estimates of >60% of burn patient deaths resulting from infectious complications (Gomez et al., 2009). Before the updated 2016 Journal of the American Medical Association (JAMA) nomenclature for sepsis (known as Sepsis-3) (Singer et al., 2016), the pathobiology was identified by the presence of two systemic inflammatory response syndrome (SIRS) criteria. However, these criteria are difficult to differentiate from the clinical manifestations of severe burns (e.g., higher white blood cell counts, temperature, and burn shock causing changes in heart rate and respiratory rate), among other clinical presentations of inflammation and host response such as compensatory anti-inflammatory response syndrome (CARS), and do not necessarily indicate the presence of infection (Chakraborty & Burns, 2023).

Several different definition-based diagnostic criteria formulations have been considered for burn patients to predict sepsis (American Burn Association (ABA)-criteria, BURN-6, FF4, Sepsis-3), however none have both high sensitivity and specificity (Hill et al., 2018; Mann-Salinas et al., 2013; Shankar-Hari et al., 2016). Current clinical practice calls for blood cultures for pathogen identification following signs of infection based on these diagnostic criteria, but this is timely, taking days for a positive result (Chela et al., 2019; Dierig et al., 2018). Investigations into clinical biomarkers of sepsis in burn patients such as cytokine and chemokine markers (interleukins (IL)-6, IL-8, IL-10), metabolites (L-lactate, procalcitonin (PCT)), soluble receptors (HLA-DR, nCD-64), and vascular endothelial cell or coagulation cascade-related markers are under investigation, but with limited viability, especially for early recognition of sepsis in this patient population (Chaudhry et al., 2013; Dal Ponte et al., 2018; Egea-Guerrero & Rodríguez-Rodríguez, 2016; Gille et al., 2021; Gregoriano et al., 2020; Lee & An, 2016; Lekkou et al., 2004; Li et al., 2022). While such investigations are ongoing, they are not clinically standard-of-care tests. There is yet to be a rapid, sensitive, and specific gold standard diagnostic criteria for burn sepsis identification (Yan et al., 2018).

Due to the heterogeneity of sepsis presentation in patients, especially in burn patients, individualized dosing of antimicrobial medication is highly important. The time-to-antibiotic treatment is imperative, with an observational study showing a 1.5% increase in mortality per hour delay of antibiotic treatment of patients in an ICU setting (Cardoso et al., 2011; Hogan et al., 2012). The timing of blood cultures for bacteraemia has a significant impact on correlation with sepsis, with positive cultures drawn at a median of 4 days after burn centre admission in a retrospective review of 282 blood cultures from 196 burn ICU patients (Hogan et al., 2012). Technical approaches for the characterization of monocyte volume in response to pro-inflammatory signals from bacteria have also not been successful in reducing lead time in sepsis detection. Thus, there is a major unmet clinical need for early-stage determination of sepsis in burn patients to ensure adequate treatment and potentially significantly improve patient outcomes.

There is a strong rationale to assess circulating extracellular vesicles (EVs) as biomarkers for sepsis due to their primary release by the pathogens involved in sepsis bacteraemia, as well as their many roles in the subsequent inflammatory response, including cell-to-cell communication. EVs are ubiquitous lipid membrane-bound nanovesicles that are secreted by all cells across all kingdoms (mammalian, plant, and bacterial) into the extracellular space (Zaborowski et al., 2015). EVs are of particular interest because their membrane-bound and internal biomolecular contents (e.g., proteins, lipids, metabolites, genetic material, cytokines) are variable in response to cellular stressors and disease pathogenesis, and can therefore be used as indicators of disease, in cancer, wound healing, neurodegenerative disorders, cardiovascular disease, and more (Fu et al., 2020; Hill, 2019; Huang et al., 2013; Narauskaitė et al., 2021; Xu et al., 2018). While EVs are central components in key cellular processes, such as contributing to homeostasis in both basic cell functions and immune response (Couch et al., 2021), intense research is underway to establish EVs as biomarkers of aberrant cell signalling and pathogenesis. EVs are widely regarded as potent candidates for liquid biopsy-based cancer detection (Ciferri et al., 2021; Xu et al., 2018). Likewise, the use of EVs for acute injury detection is growing with potential applications cited for sepsis, making EV diagnostics for early detection of sepsis a viable option for routine patient care (Tian et al., 2022).

In prokaryotes, EVs were originally thought to be produced by gram-negative bacteria, so-called outer membrane vesicles (OMVs), then 30 years after their initial discovery, reports of EVs produced by gram-positive bacteria surfaced (Bishop & Work, 1965; Deatherage & Cookson, 2012; Dorward & Garon, 1990). Thus, identifying EVs released by microbial cells driving infection in burn patient populations is of particular interest, since they may be released in high numbers into circulating biofluids via damaged endothelium at the site of burn injury (Figure 1a).

Here we apply label-free Raman spectroscopy (RS) to analyze circulating EVs isolated from patient plasma. RS is a non-destructive, label-free optical spectroscopic method that captures a comprehensive snapshot of the chemical composition of a given biofluid, whereby the signal reflects the complex mixture of lipids, metabolites, proteins, and more in each sample based on changes in their molecular vibrations (Nottingham et al., 2003; Pappas et al., 2000; Raman, 1929). Chemical spectroscopic analysis of EVs using RS has recently shown great promise as a label-free tool with high sensitivity to detect and monitor disease in a variety of contexts, particularly in liquid biopsy analysis (Koster et al., 2021). Several studies have investigated the application of RS to distinguish bacterial EVs released from different pathogen sources (Horgan et al., 2020;

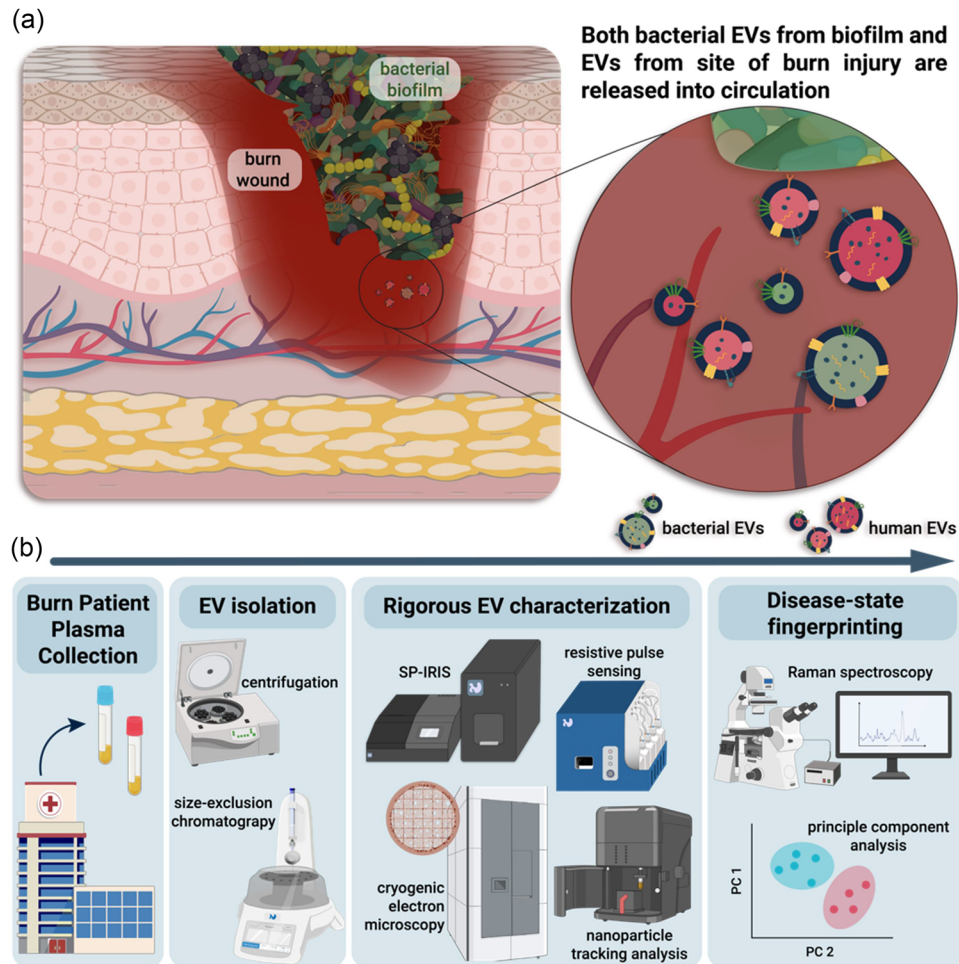


**FIGURE 1** Extracellular vesicle release during bacterial infection in burn injury; Overview schema of sample preparation and acquisition. (a) The rationale behind our work is that EVs originating from colonizing bacteria are released into circulatory biofluids via damaged endothelium at the site of burn injury. Inflammatory response to injury results in secondary release of EVs from immune and endothelial cells as well. (b) Collection and analysis of EVs in circulating biofluids are a way to determine sepsis in advance of currently available methods.

Kazemzadeh et al., 2022; Qin et al., 2022). We utilize this approach to establish a comprehensive workflow to evaluate EV liquid biopsy isolated from burn patient plasma samples as a proof-of-concept for sensitive and rapid detection of sepsis (Figure 1b).

## 2 | RESULTS AND DISCUSSION

### 2.1 | Clinical biofluid collection

De-identified remnant clinical chemistry lithium heparin plasma samples were collected from adult burn patients from the University of California, Davis Health Fire Fighters Burn Institute Regional Burn Centre. Samples utilized the UC Davis Pathology Biorepository anonymous clinical research specimen (ARCS) protocol (IRB#1911992). Further information is described in the Methods section.

In this study, patient plasma from both septic and non-septic burn patients was analysed ( $n = 14$ ). Patient samples were collected the same day that each patient met the ABA burn sepsis criteria, and microbiology samples were collected, which later became positive in the case of septic burn patients. During the course of our study of these remnant clinical chemistry samples, two of the patients' prognoses were updated, and they were included within the septic burn patient sample cohort ( $n = 8$ ) for analysis. Available de-identified patient information is summarized in Table S1, including age, sex, procalcitonin level, and total body surface area (TBSA) of burn. The average TBSA (%) for each patient population was  $34.8\% \pm 11.4\%$  for septic burn patients

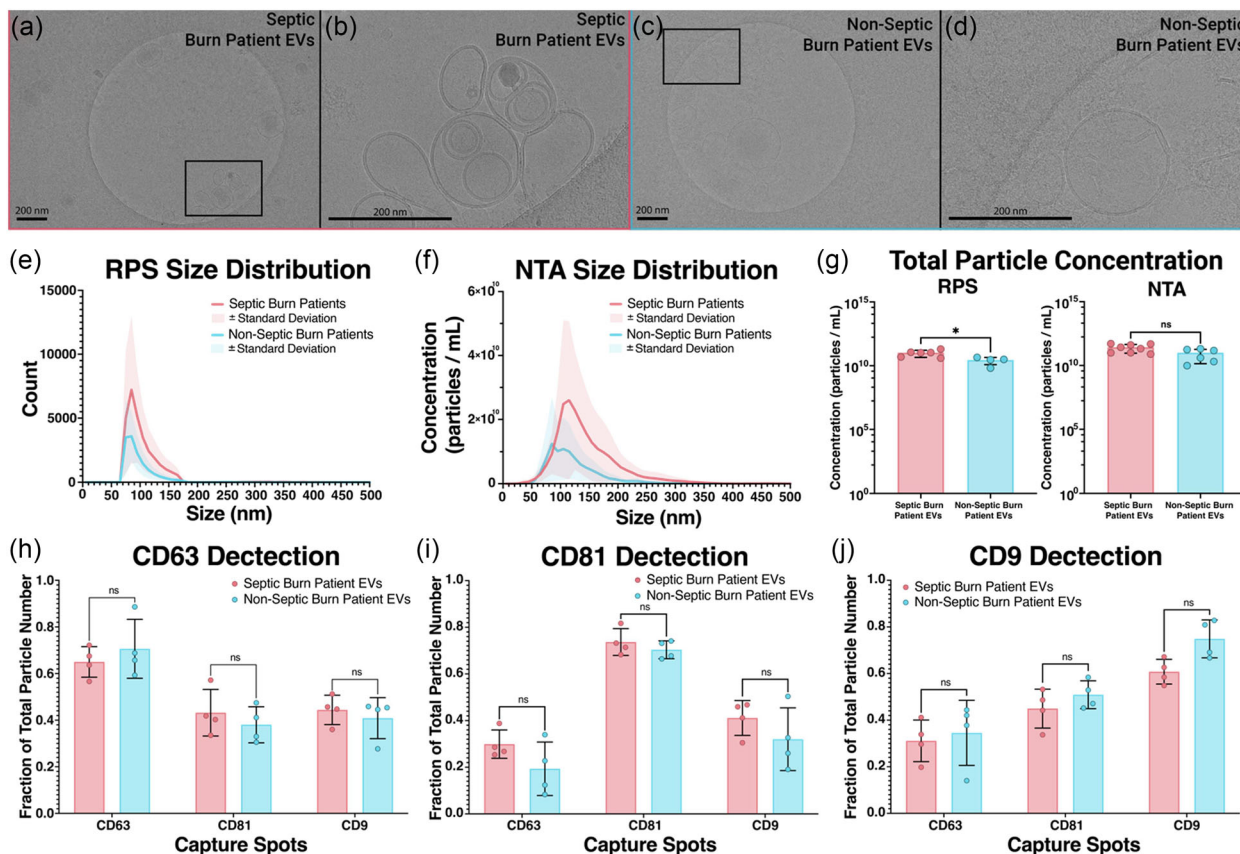


**FIGURE 2** Characterization of SEC isolated EVs from septic and non-septic burn patient plasma. (a–d) CryoEM images of isolated EVs from (a, b) septic and (c, d) non-septic burn patient samples reveal the expected lipid bilayer structure. Images were acquired at (a, c) 11k and (b, d) 45k magnification. Scale bars are 200 nm. (e) RPS and (f) NTA were used to determine the average size distribution of the EVs isolated from the septic and non-septic burn patient samples. Shaded regions designate size standard deviations (g). The total EV particle concentration of the samples was measured by RPS and NTA. (h–j) The presence and co-localization of human EV biomarkers (h) CD63, (i) CD81, and (j) CD9 were determined by an immunofluorescent tetraspanin kit assay using ExoView.

and  $24.4 \pm 2.3\%$  for non-septic burn patients. The average TBSA across both patient populations was  $30.4\% \pm 10.9\%$ . It is of note that burns  $>20\%$ – $25\%$  TBSA require IV fluid resuscitation and burns  $>30\%$ – $40\%$  TBSA may be fatal if untreated (Burn Triage and Treatment—Thermal Injuries—CHEMM).

## 2.2 | EV isolation and characterization

We first isolated and characterized EVs from patient plasma samples ( $n = 14$ ). Patient plasma was centrifuged to remove cell debris. Size exclusion chromatography (SEC) was then used to isolate EVs from septic ( $n = 8$ ) and non-septic ( $n = 6$ ) burn patient plasma samples. EVs were subsequently characterized by morphology and size, following suggestions from the Minimal Information for Studying Extracellular Vesicles (MISEV) 2023 guidelines and technique-specific recommendations for EV characterization as shown in Figure 2 (Théry et al., 2018; Welsh et al., 2024). As suggested by MISEV 2023, EV morphology was further characterized with cryogenic electron microscopy (CryoEM) as a complementary method. CryoEM images of the EVs reveal the expected lipid bilayer structure for both septic and non-septic samples (Figure 2a–d).

Resistive pulse sensing (RPS) and nanoparticle tracking analysis (NTA) were used to determine the EV size distributions (Figures 2e–f and S1). We found the average diameter of the septic burn patient EV samples to be  $103.59 \pm 0.28$  nm (mean  $\pm$  SE) and  $141.46 \pm 14.66$  nm (mean  $\pm$  SD) for RPS and NTA, respectively. This is compared to the non-septic burn patient samples with an average diameter of  $98.13 \pm 0.28$  nm (mean  $\pm$  SE) and  $130.07 \pm 15.29$  nm (mean  $\pm$  SD) for RPS and NTA, respectively. The difference in average diameter between EVs isolated from septic and non-septic burn patient samples was statistically significant for the NTA measurement (unpaired  $t$ -test,  $p = 0.0032$ ). The NTA size distribution is a bell-shaped curve due to the limit of detection of EVs on NTA ( $\sim 80$  nm) and the low light-scattering efficiency of EVs (Bachurski et al., 2019). On the other hand, the RPS size distribution shows a sharper peak near its respective limit of detection of  $\sim 65$  nm.

RPS and NTA were also utilized to determine the total concentration of particles isolated from the samples (Figure 2g). The average concentration of particles isolated from septic burn patient EV samples were  $1.02 \times 10^{11}$  and  $2.68 \times 10^{11}$  particles per millilitre for RPS and NTA, respectively. The average concentration for non-septic burn patient EV samples was  $2.78 \times 10^{10}$  and  $9.90 \times 10^{10}$  particles per millilitre for RPS and NTA, respectively. EVs isolated from the septic burn patient samples had statistically significantly higher concentrations compared to those from the non-septic burn patients as determined by RPS (unpaired *t*-test,  $p = 0.0383$ ). While a similar trend was seen for concentration measured by NTA, no statistically significant difference was found ( $p = 0.0523$ ). It is possible that this increase in concentration between septic and non-septic burn patient EVs is related to the relative bacterial load of EVs between the two populations. Differences in concentrations between NTA and RPS measurement methods may be attributed to the presence of EVs smaller than the limit of detection of NTA versus RPS (Bachurski et al., 2019).

The presence and co-localization of human EV biomarkers CD63, CD81, and CD9 in isolates were confirmed using an immunofluorescent tetraspanin kit assay (Figures 2h–i and S1). No significant difference in tetraspanin expression was observed between the two EV populations (unpaired *t*-test,  $p > 0.05$ ). Tetraspanin expression was measured with the immunofluorescent tetraspanin kit assays using microarrayed chips with antibody capture spots for human CD63, CD9, and CD81. It is of note that neither bacteria nor their EVs express these tetraspanins, although they do interact with them (Green et al., 2011; Hemler, 2005; Karam et al., 2020). Therefore, the tetraspanin kit assays would not capture bacterial EVs, and the observed difference in RPS measured concentration may be attributed to measuring additional EVs secreted from bacteria and/or due to patient secretion of EVs in response to infection. Guidance on bacterial EV-specific markers or other characterization methods was not published at the time of data collection (e.g., MISEV 2018), and is limited to broad glycoconjugate markers like LTA and LPS for gram-positive and gram-negative bacterial classes respectively as recommendations from the updated MISEV 2023 (Théry et al., 2018; Welsh et al., 2024).

### 2.3 | Raman spectral differences between septic and non-septic burn patient EVs

Following isolation and characterization of the EVs isolated from patient plasma, analysis via spontaneous Raman spectroscopy was performed. Burn patients were used as the control population in this study due to the overlapping clinical manifestations that burn patients and septic burn patients share in comparison to other patient populations (e.g., ill patients who have a topical bacterial infection that is not considered septic, or healthy controls). Comparison of the spontaneous Raman spectral profiles of EVs isolated from septic burn patients to non-septic burn patients represents a more realistic diagnostic scenario than comparison to healthy controls for this utilization case, where the standard diagnostic criteria fail to be upheld.

Spontaneous Raman spectroscopic analysis was performed on the EV patient samples ( $n = 8$  septic burn patients and  $n = 6$  non-septic burn patients as controls). A 2  $\mu$ L drop of each EV sample was deposited onto a quartz coverslip, dried, and analysed on a custom-built inverted Raman microscope. A quick (90 s) spectral acquisition was performed for each sample at five different spots along the outer coffee ring of the dried sample, where EVs tend to be enriched (Jeong et al., 2018, 2019). Global spectral averages for septic versus control burn patients and their standard deviations are shown in Figure 3a. To investigate the differences between these patient population EV spectral profiles, we subtracted the spectral averages in MATLAB, where the difference between population averages =  $\text{mean}_{\text{septic\_patients}} - \text{mean}_{\text{non-septic\_patients}}$ . The remnant spectrum of the difference between population averages is shown in Figure 3b. Positive peak intensities correlate to a higher normalized intensity of that peak in the septic burn patient EV average Raman spectrum, whereas negative intensities indicate a higher normalized intensity of that peak in the non-septic burn patient EV average spectrum.

Notable spectral differences include: an increased peak intensity at  $718 \text{ cm}^{-1}$  associated with  $\text{CN}^+(\text{CH}_3)_3$  stretching in the head group of phosphatidylcholine, an increased peak intensity at  $877 \text{ cm}^{-1}$  associated with  $\text{C—C—N}^+$  symmetric stretching in lipids and  $\text{C—O—C}$  ring vibrations in carbohydrates, a decreased peak intensity at  $1005 \text{ cm}^{-1}$  associated with the symmetric ring breathing of phenylalanine in proteins, increased peak intensities at  $1068 \text{ cm}^{-1}$  and  $1095 \text{ cm}^{-1}$ , associated with  $\text{PO}_2^-$  stretching in DNA and RNA, a decreased peak intensity at  $1253 \text{ cm}^{-1}$  in the Amide III region in the secondary structures of proteins, an increased peak intensity at  $1301 \text{ cm}^{-1}$  associated with the  $\text{CH}_2$  twisting mode in lipids, an increase at  $1380 \text{ cm}^{-1}$  correlated to RNA hairpins, an increase in  $\text{C—H}$  vibrations at  $1440 \text{ cm}^{-1}$  associated with the  $\text{C—H}$  bonds found across biological molecules, decreased intensity at  $1535 \text{ cm}^{-1}$  attributed to asymmetric  $\text{NO}_2$  stretch in the presence of a benzene ring, and the presence of a slight increase at  $1731 \text{ cm}^{-1}$  resulting from carbonyl stretching vibrations (Hauptmann et al., 2023; Hobro et al., 2007; Notingher, 2007; Nyquist, 1971).

### 2.4 | Differences in EV spectral profiles enable discrimination via PCA/QDA

To evaluate the utility of spontaneous Raman spectra of patient EVs as a proof-of-concept clinical indicator of sepsis in burn patients, we performed principal component analysis (PCA) and multivariate discriminant analysis. Raman spectral data were cropped, smoothed, and normalized using established methods (Eilers, 2003; Stähle & Wold, 1987; Whittaker, 1922; Zhang et al.,

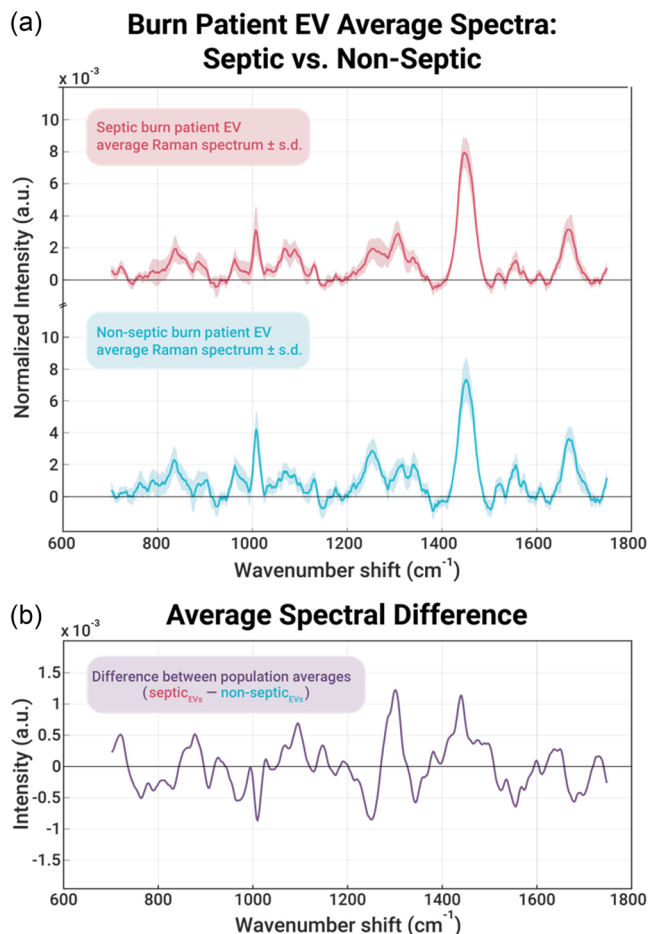


**FIGURE 3** Global averages of septic and non-septic burn patient EVs. (a) Normalized global average and standard deviation spontaneous Raman spectra for septic burn patient EVs ( $n = 8$ ) (a), and for control non-septic burn patient EVs ( $n = 6$ ). For each patient plasma-isolated EV sample, a 90s spectrum was acquired at five different spots. (b) The normalized spectral difference between septic and non-septic burn patients Raman global average spectrum.

2010). Normalization and PCA permitted dimensionality reduction of our dataset and limited feature scale sensitivity (Randolph, 2006). Spectral data stacks were created for both the spectra acquired from the septic burn patient EV samples and for the non-septic burn patient EV samples. Figure 4a visualizes the individual patient spectra plotted in 2D-PC space along PC1 and PC2, encompassing nearly half (49.2%) of the total variance of the dataset.

We performed supervised discriminant analytical data analysis to better visualize and model the separation of septic burn patients from non-septic (control) burn patients. Every combination of the first five principal components (PCs) (chosen as they represent  $> 70\%$  of the cumulative variance) was run through a custom MATLAB script to select the best data visualization model included within built-in MATLAB classifiers. PC loading coefficients are shown in Figure S2a–e.

Quadratic discriminant analysis (QDA) of the first five PCs (PC1–PC5), accounting for 72.2% of the total cumulative percent variance, resulted in the highest combination of accuracy, sensitivity, and specificity of the patient clinical classifications (Figure 4b). With this classifier, we have achieved 97.5% sensitivity and 90.0% specificity, with 94.3% accuracy in fitting the Raman spectra of the EV samples into PC space. Of the 70 patient spectra collected and passed through the classifier, just one was falsely predicted as non-septic and three were falsely predicted as septic, yielding a 2.5% false negative rate and a 10% false positive rate. A visual representation of the 70 measured spectra plotted in three-dimensional PC space (PCs 1–3), along with the quadratic hyperplane of best fit can be found in Figure S2f.

While QDA analysis of the PC space caused a 10% incidence of false positives (Type I error), it is notable that the false negative rate is low (2.5%) (Type II error). In this particular clinical indication, it is of the utmost importance to detect, and then treat, septic burn patients as soon as possible. There are minimal effects of treating patients with antibiotics who ultimately do not prove to be septic (i.e., false positive), however, it is critical that patients who are at risk of becoming, or already are, septic get the antimicrobial treatment, resources, and timely care they need to better their prognosis (Avni et al., 2010). Furthermore, sensitive, rapid identification of the bacteria present would help guide specific clinical treatment, lessening the need and time for systemic

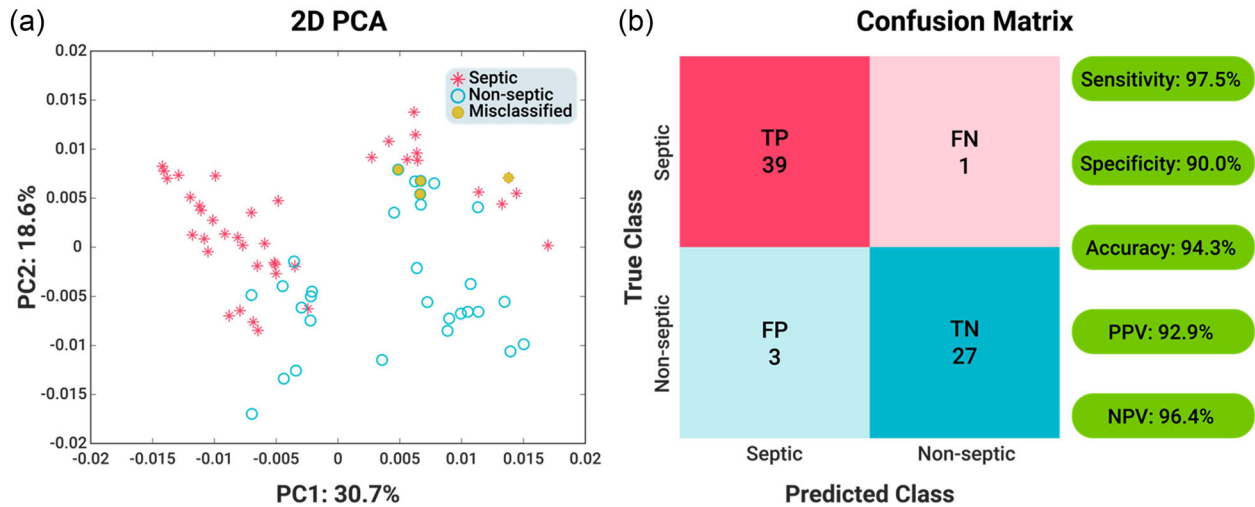


**FIGURE 4** Principal component analysis and confusion matrix results. (a) Normalized spontaneous Raman spectra acquired from patient EV samples ( $n = 70$ ) underwent principal component analysis and are plotted in PC space along PC1 and PC2. This 2D PC space encompasses 49.2% of the total variance of the dataset. Septic burn patient spectra are shown as pink stars, and non-septic control burn patients are labelled as blue circles. QDA analysis incorrectly identified four spectra, shown in a yellow overlay on their respective marker. Three spectra were found to be from the same non-septic burn patient (ARCS barcode number 1879), which were misclassified as septic (false positive, FP). One spectrum from a septic burn-patient was misclassified as non-septic (false negative, FN). (b) A confusion matrix visualizes the output of the optimized QDA analysis across the first five PCs (PC1–PC5). Notably, just one of the 70 spectra was classified as a false negative result, yielding a high negative predictive value of 96.4% and a high sensitivity of 97.5%.

prophylactic antibiotics and potentially reducing the risk of downstream antibiotic resistance (Avni et al., 2010). In this case, the trade-off between sensitivity versus specificity of detection favours sensitivity. Thus, our higher negative predictive value and low false negative rate support the premise of using spectral differences in the EV Raman fingerprint isolated from patient plasma samples.

For comparison, the use of procalcitonin (PCT) as a biomarker for sepsis in burn patients showed 82% sensitivity and 91% specificity following initial burn trauma but decreased to a combined 67% sensitivity and 87% specificity after this initial trauma phase, similar to the state of the patients in this study, as reported in a 2021 meta-analysis (Chen et al., 2021; Lavrentieva et al., 2007). While there has been interest in IL-6 and IL-10 as biomarkers of sepsis in burn patients, they still do not have sufficient sensitivity and specificity for clinical use (79.5% sensitivity and 56.5% specificity in the case of IL-6 levels in serum) and are not FDA approved in the United States for clinical care (Gille et al., 2021; Pileri et al., 2008). Thus, our methodology shows promise for improving sensitivity and specificity when compared to current biomarkers of sepsis in burn patients.

Interestingly, three of the four misclassified spectra of the 70 acquired were from the same patient (ARCS patient barcode 1879), contributing to the Type I error, false positive. Spectral misclassifications could be interesting to examine with a larger data pool, to investigate other clinical indications or patient background information that could be driving the misclassifications. Exploring whether misclassifications correlate with specific patient comorbidities or treatment regimens could provide valuable information for personalized diagnostic approaches.

## 2.5 | Differences in patient EV Raman spectra are in part driven by the presence of bacterial EV glycoconjugate biomarkers

Common bacterial strains associated with septic bacteraemia in both burn and non-burn patients include Gram-negative bacteria such as *Klebsiella* spp., *Escherichia coli*, and *Pseudomonas aeruginosa*, as well as Gram-positive organisms including *Staphylococcus aureus* and *Streptococcus* spp., among others (Church et al., 2006; Fournier & Philpott, 2005; Ramachandran, 2014). Since 1987, gram-positive bacteria have arisen as the predominant pathogens responsible for sepsis in the United States (Martin et al., 2003).

We hypothesized that the spectral differences of septic versus non-septic burn patient EVs would be at least in part driven by the presence of pathogenic bacterial EVs shed from bacterial biofilm into the bloodstream. Thus, we sought to identify spectral markers of these bacteria-derived EVs to explain the Raman spectral differences of the EVs isolated from our two patient populations. The different biogenesis pathways of bacterially derived EVs cause them to have membrane glycoconjugate biomarkers.



**TABLE 1** Characteristics of chosen bacterial glycoconjugate biomarkers.

Glycoconjugate	Associated bacteria	Gram stain	Origin	Purpose	Structure and features	Role in sepsis
Lipopolysaccharides (LPSs)	<i>E. coli</i>	–	Outer leaflet of asymmetric outer membrane bilayer of Gram-negative bacteria. Exposed to cell surface in <i>E. coli</i> and <i>P. aeruginosa</i> , and below capsular layer in <i>K. pneumoniae</i>	Maintain outer membrane barrier structure to protect bacteria from passive diffusion of antibiotics and detergents like bile salts. LPSs are inherent to Gram-negative bacteria.	<ul style="list-style-type: none"> <li>Lipid A, a hydrophobic endotoxin; anchors to outer membrane</li> <li>O-antigen, a hydrophilic distal oligosaccharide; serological distinction for bacterial species; impacts virulence</li> <li>Distal core hydrophilic non-repeating polysaccharide; maintains membrane integrity</li> </ul>	<ul style="list-style-type: none"> <li>Recognized as pathogen-associated molecular pattern (PAMP) by toll-like receptor 4 (TLR4)</li> <li>Lipid A induces host innate immune response and the coagulation cascade through binding to CD14/TLR4/MD2 receptor complexes on host immune cells</li> <li>Promotes bacterial biofilm formation</li> </ul>
	<i>P. aeruginosa</i>	–				
	<i>K. pneumoniae</i>	–				
Lipoteichoic acid (LTA)	<i>S. aureus</i>	+	Capsular polysaccharide (CPS), the outermost layer of most Gram-Positive bacterial cell walls	Protection against cationic antimicrobial peptides	<ul style="list-style-type: none"> <li>Decorated with Phosphoryl choline (ChoP)</li> <li>Highly cationic polymers</li> <li>Polyglycerol phosphate (poly(Gro-P)) repeating chain</li> </ul>	<ul style="list-style-type: none"> <li>Provokes secretion cytokines and chemo-attractants from monocytes or macrophages of host innate immune system</li> <li>Initiates recruitment of phagocytes to infection</li> </ul>

Briefly, bacterial EV (bEV) biogenesis is dependent on the group of bacteria they are derived from. Gram-negative bacterial EVs are commonly referred to as outer membrane vesicles (OMVs), and their biogenesis has been thought to be due to release from the outer membrane via reduction of outer membrane peptidoglycan–protein linkages, differential assembly of lipids/lipopolysaccharides (LPS) into microdomains, swelling pressure due to protein or peptidoglycan accumulation, or by explosive cell lysis (Tian et al., 2023). Gram-positive bEVs come about differently, due to the thick outer peptidoglycan layer of the bacterial cell cytoplasmic membrane complete with polyanionic matrix polymers such as macro amphiphiles like lipoteichoic acid (LTA), as well as the lack of outer membrane structure that gram-negative bacterial cells possess (Neuhaus & Baddiley, 2003; Tian et al., 2023). The different bEV biogenesis pathways effectively create vast heterogeneity within bEV/OMV types, however, there are some distinguishing characteristics between them such as their bacterial glycoconjugates. Glycoconjugates are glycans with covalently linked species such as peptides, lipids, proteins, etc. We chose to investigate glycoconjugate markers for bacterial strains commonly associated with sepsis in burn patients. These bacterial glycoconjugates and their origins are further described in Table 1 (Farhana & Khan, 2024; Fournier & Philpott, 2005; Gabarin et al., 2021; Ramachandran, 2014; Schneewind & Missiakas, 2014; von Aulock et al., 2003).

It has been shown that discrete differences between enteric LPSs isolated from several gram-negative bacterial strains can be revealed through a comparison of normalized surface-enhanced Raman scattering (SERS) spectra (Wu et al., 2021). Thus, to assess whether the spectral differences we noted in this study were at least in part driven by the presence of bacterial EV signatures, we measured lyophilized powder LPS analytical standards from *E. coli*, *K. pneumoniae*, *P. aeruginosa*, and an LTA analytical standard isolated from *S. aureus* (more information found in the Methods section). Raman spectra for each bacterial glycoconjugate standard were acquired with four replicates. These spectra were then normalized, smoothed, and background corrected for analysis.

To demonstrate that there are indeed unique spectral differences between these bacterial glycoconjugates that can be elucidated with spontaneous Raman, we performed PCA and hierarchical clustering. Clear spectral variance between each of these glycoconjugate standards was observed by their distinct hierarchical clustering in 3D PC space, as shown in Figure 5a. The generated average spectrum of the four replicates for each chosen glycoconjugate analytical standard after normalization, smoothing, and PLS fitting are shown in Figure 5b. After confirming discrete spectral differences between the glycoconjugate analytical standards, we compared them to the spectral difference of the population average spectra of septic and non-septic burn patient EVs (Figure 3b). The asymmetric least squares fit of these standards to the difference between population averages Raman spectrum is shown in Figure 5c.

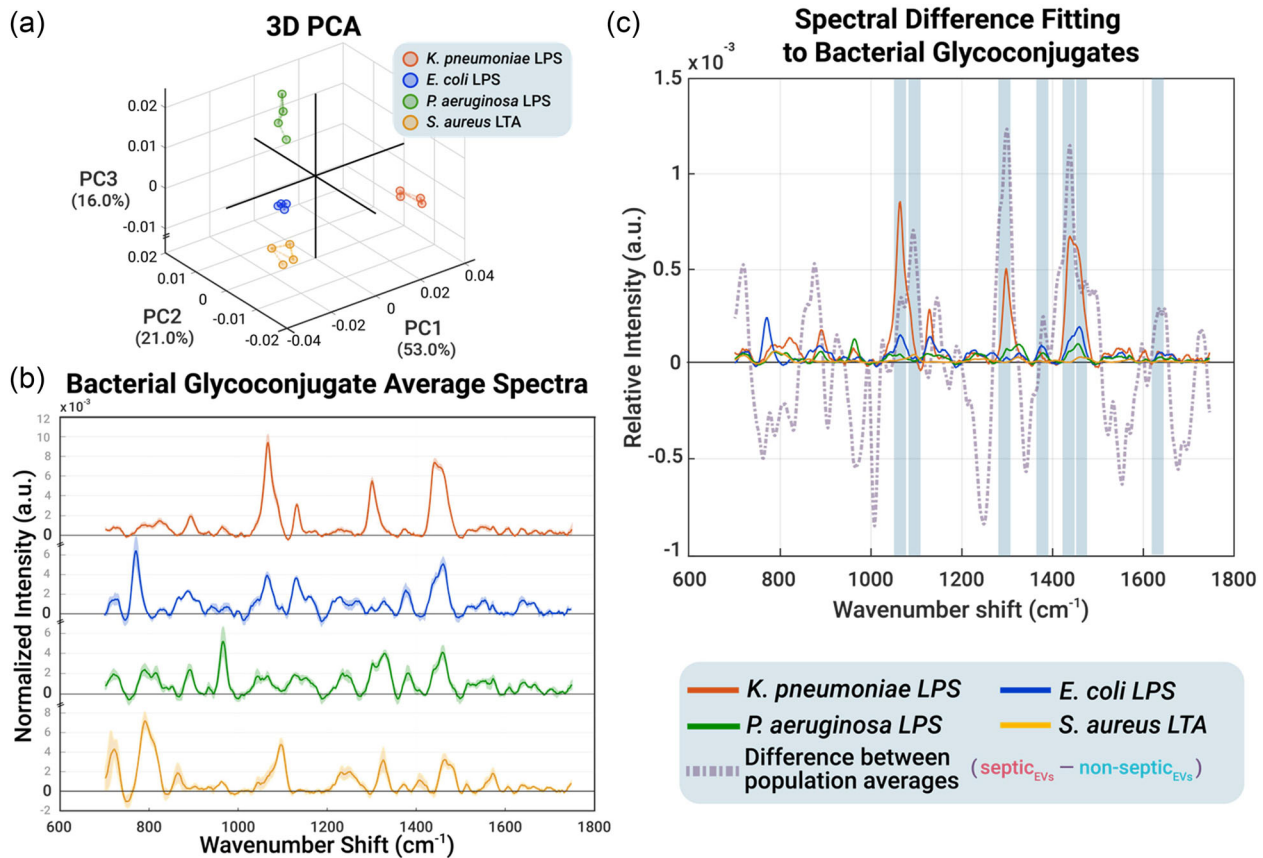


**FIGURE 5** Utilizing bacterial glycoconjugates to elucidate spectral differences between septic and non-septic burn patient EV Raman fingerprints. (a) Clustering analysis of the four chosen bacterial glycoconjugates' Raman spectra visualized in three-dimensional principal component space across the first three PCs, accounting for 90% of the variance. Clear clustering validates spectral differences between the four standards for downstream use as reference analytes. (b) The average spontaneous Raman spectrum of each chosen bacterial glycoconjugate analytical standard following normalization, smoothing, and PLS fitting. Each standard was measured four times then averaged. Shading shows the standard deviation. (c) Comparison of the difference of the average spectrum of non-septic burn patient EVs from septic burn patient EVs (denoted as difference between population averages, in purple) to the four chosen bacterial glycoconjugates of bacteria commonly associated with sepsis in burn patients. Raman band fits are highlighted in blue. Key in bottom right corner of figure is for panels (b) and (c).

While there are some clear feature overlaps with the sepsis-related EV spectral features to the bacterial glycoconjugate standards, there is not one overwhelmingly strong fit. Spectral peak fitting shows some overlap with lipopolysaccharides isolated from *K. pneumoniae*, *E. coli*, and *P. aeruginosa*, respectively. Fit with *S. aureus* LTA was only observed at  $1095 \text{ cm}^{-1}$ . These results are summarized in Table 2 (Osorio-Román et al., 2010; Schneewind & Missiakas, 2014; Wu et al., 2021; Yang et al., 2022). Understandably, the total variance between the Raman signatures of the two EV populations would not be fully explained by these four specific bacterial glycoconjugates (Welsh et al., 2024). Investigation into spectral fitting to the LTA glycoconjugate from *Streptococcus pyogenes* was also performed but did not yield any notable overlap, potentially because the patients in this study may not have had sepsis caused by Group A *Streptococcus* (Figure S3).

Other work has investigated SERS spectral classification of bacterial EVs from *E. coli* strains, as well as SERS for six typical bacteria contributing to nosocomial infections, however, there has yet to be a study into spontaneous Raman of bacterial EVs isolated from patient biofluids (Kazemzadeh et al., 2022; Qin et al., 2022). Differentiation of systemic inflammatory response syndrome and sepsis from plasma using Raman spectroscopy has been reported, but was not specific to sepsis in burn patients and did not investigate the roles of bacteria, EVs, or bacterial EV signatures (Neugebauer et al., 2014).

The field of bacterial EV characterization still requires further advancement. Specific biomarkers for bacteria-derived EVs have yet to be identified and agreed upon, and RS-based EV characterization is still in its infancy, thus large datasets for comparison across studies are not available (Welsh et al., 2024). Differential underlying patient microbiota or different pathogenic bacterial strains may also be a driving contribution to the spectral separation and are fields of interest for future study (Pope et al., 2017; Wang et al., 2020).

Ultimately, while these results are promising, limitations of our work include a low patient number due to the niche patient population, precluding more advanced deep learning to improve model performance. The relatively small sample

**TABLE 2** Fits for Raman spectra of bacterial glycoconjugates to the difference of population average spectrum.

Raman band	Vibrational mode and assignment	Associated glycoconjugate(s)
1067 $\text{cm}^{-1}$	C—C and C—O stretching vibrations of O-antigen and distal LPS core (Mangini et al., 2021)	<i>K. pneumoniae</i> LPS <i>E. coli</i> LPS
1095 $\text{cm}^{-1}$	P—O stretching of poly(Gro-P) chain (Schneewind & Missiakas, 2014)	<i>S. aureus</i> LTA
1301 $\text{cm}^{-1}$	C—H deformation and $\text{CH}_2$ bending of O-antigen and distal LPS core (Mangini et al., 2021)	<i>K. pneumoniae</i> LPS <i>E. coli</i> LPS <i>P. aeruginosa</i> LPS
1380 $\text{cm}^{-1}$	$\text{CH}_3$ deformation and C—N stretching in O-antigen (Yang et al., 2022)	<i>K. pneumoniae</i> LPS <i>E. coli</i> LPS
1440 $\text{cm}^{-1}$	$\text{CH}_2$ scissoring in lipid A (Yang et al., 2022)	<i>K. pneumoniae</i> LPS <i>E. coli</i> LPS <i>P. aeruginosa</i> LPS
1455 $\text{cm}^{-1}$	$\text{CH}_2/\text{CH}_3$ scissoring, C—O—C deformation in glycosidic linkages, C—C—C deformation, and C—O—H deformation in lipid A (Yang et al., 2022)	<i>P. aeruginosa</i> LPS
1637 $\text{cm}^{-1}$	C—O and C—C stretching within lipid A (Yang et al., 2022)	<i>K. pneumoniae</i> LPS <i>E. coli</i> LPS

size of the study is further attributed to the use of remnant plasma samples derived from routine clinical chemistry samples drawn at regular intervals, rather than at the time of initial sepsis diagnosis. As aforementioned, samples used were acquired when patients met ABA criteria for burn sepsis, and the presence of sepsis was confirmed at later time points with positive microbiology testing. Other potential limitations in the burn population are the aforementioned difficulties in the identification of sepsis, as burn patients exhibit inflammatory response syndrome throughout their hospitalization. Burn patients may also exhibit transient bacteraemia from dressing changes and/or surgical excision of heavily colonized wounds. An early marker that distinguishes these different states, such as the EV-Raman workflow described in this work, will help to move the science of sepsis forward. Further prospective collection of samples and associated clinical outcomes will build on this work.

Nevertheless, we recognize the utility and translatability of RS analysis of EVs for the detection and diagnosis of other bacterial bloodstream infections. For example, staph infections, caused by the gram-negative bacteria *S. aureus*, have a mortality rate of around 30% (van der Vaart et al., 2022). Current diagnostic methods rely on culture-based methods spanning multiple days, or genomic/proteomic methods which require highly specialized equipment and technicians (Dahal & Schwan, 2018; Jenkins & Bean, 2023). Earlier diagnosis of staph infection has been shown to decrease relative mortality by 75.5% (Bouza et al., 2020). Therefore, employing a similar workflow to that described in this work for early diagnosis of staph infection via RS could be used to decrease the mortality of patients. Raman EV analysis could also be translated to the diagnosis of other infectious diseases caused by bacteria. In 2021, 1.6 million people died of tuberculosis (TB) caused by *M. tuberculosis*. Efficient diagnosis of TB is critical for effective treatment of TB, which is estimated to have saved 74 million lives from 2000 to 2021 (Gill et al., 2022; Tuberculosis (TB)). EVs secreted by *M. tuberculosis* bacteria have been established as a reliable biomarker of TB and therefore Raman EV analysis following our workflow may be useful for diagnosis of TB (Jnana et al., 2023).

### 3 | CONCLUSION

The focus of this work was to utilize Raman spectroscopy to spectrally discriminate markers of sepsis in EVs isolated from burn patient plasma. We show, for the first time, the possibility of utilizing spontaneous Raman scattering and resultant spectra of patient plasma-isolated extracellular vesicles for the rapid detection of sepsis in burn patients. This workflow, from collection to analysis, can be completed in an hour, in comparison with the 2–3 days needed for a positive bacterial culture confirmation of sepsis in burn patients. Furthermore, quadratic discriminant analysis of the acquired patient EV Raman spectra separated septic from non-septic burn patient EVs with 97.5% specificity and 90.0% sensitivity, beating current investigations into other biomarkers of sepsis in this patient population. We also were able to, in part, attribute the spectral differences to the presence of bacterial EV markers of four common bacterial strains that contribute to sepsis morbidity such as lipopolysaccharides for *K. pneumoniae*, *E. coli*, and *P. aeruginosa*, and lipoteichoic acid isolated from *S. aureus*. Overall, we contributed to the discourse surrounding bEVs and OMVs for pathogenic detection, but there is still much work to be explored in this field regarding their isolation and characterization. Collectively, our proof-of-concept findings establish a rapid, sensitive workflow for future clinical

applications of spectral investigation into bacterial EVs within host biofluids and show the promise of Raman spectroscopy of patient plasma-isolated EVs for early identification and stratification of sepsis in vulnerable burn patient populations.

## 4 | METHODS

### 4.1 | Patient plasma sample collection

Both control (non-septic) and septic de-identified remnant clinical chemistry lithium heparin patient plasma samples were provided by the University of California, Davis Pathology Biorepository. Samples were derived from residual clinical chemistry plasma samples collected from adult burn patients at the burn intensive care unit (BICU) at the University of California, Davis Health Fire Fighters Burn Institute Regional Burn Center. Initial samples were collected the same day that each patient met the American Burn Association burn sepsis criteria, along with microbiology samples that later confirmed sepsis (if positive, in the case of septic burn patients). No patients were on any pharmaceutical immunosuppressants. There were no exclusion criteria to the sample collection other than non-admission for skin injuries other than burns, prisoners, or pregnant patients. Samples were collected in accordance with the UC Davis Institutional Review Board (IRB #1911992) and utilized the UC Davis Pathology Biorepository anonymous clinical research specimen protocol. Under the ARCS, only patient demographics such as age, gender, race/ethnicity, quality of specimen, collection container, etc. are available to the researcher. Patient data is stripped of identifiers and assigned an ARCS barcode number. Available patient data is summarized in Table S1.

### 4.2 | EV isolation

We have submitted all relevant data of our experiments to the EV-TRACK knowledgebase (EV-TRACK ID: EV240151) (Van Deun et al., 2017). All work with EVs was performed utilizing Protein Lo-Bind Eppendorf tubes (Catalogue No. 022431081, Eppendorf; DE), and Lo-Bind pipette tips (Corning DeckWorks, Corning Inc.; NY, USA). Plasma from control and sepsis patients was centrifuged in Protein Lo-Bind Eppendorf tubes (Catalogue No. 022431081, Eppendorf; DE) at 5000  $\times g$  for 10 min to remove cells and cell debris. The supernatant was collected and stored at  $-80^{\circ}\text{C}$  until further isolation. Izon qEV single 35 nm SEC columns and automatic fraction collector (AFC) v2 with firmware version v1.3.1 were then used to isolate the EVs (Izon Science Ltd; NZ). The column storage buffer was removed and 6 mL of 0.2  $\mu\text{m}$  filtered PBS was used to flush the columns. About 100  $\mu\text{L}$  of sample was added to the column followed by 3 mL of 0.2  $\mu\text{m}$  filtered PBS after the sample moved through the column frit. If samples needed to be diluted to reach this 100  $\mu\text{L}$  volume, they were diluted in 0.2  $\mu\text{m}$  filtered PBS. A single fraction of 0.8 mL was collected after collecting an initial buffer volume of 0.87 mL. The collected fraction was aliquoted to prevent freeze-thaw cycling and stored at  $-80^{\circ}\text{C}$  until further analysis was performed. Columns were not re-used.

### 4.3 | CryoEM

Copper grids (Quantifoil, 1.2  $\mu\text{m}$  diameter holes, 1.3  $\mu\text{m}$  separation, 300 M Cu grid) were glow discharged for 25 s at 15 mA negative polarity (PELCO easiGlow, Ted Pella Inc.; CA, USA). The grids were then loaded onto the Leica EM GP2 Plunge Freezer (Leica Microsystems Inc., IL, USA). The chamber was kept at  $18^{\circ}\text{C}$  and 80% humidity, and the cryogen was kept at  $-180^{\circ}\text{C}$ . About 4  $\mu\text{L}$  of sample was then incubated onto the grid for 2 min, blotted for 6 s, then flash frozen. Grids were stored in liquid nitrogen until imaged. Imaging of the grids was performed on a FEI Talos L120C Transmission Electron Microscope (Thermo Fisher Scientific Field Electron and Ion Company (FEI); OR, USA). Images were analysed using Adobe Photoshop 2023 (version 24.4.1, Adobe; CA, USA) and contrast was increased to 100.

### 4.4 | Nanoparticle tracking analysis (NTA)

Nanoparticle tracking analysis (NTA) was performed using a NanoSight model LM10 (Malvern Panalytical Ltd.; UK), equipped with a 405 nm laser and sCMOS camera. SEC-isolated EV samples were thawed at room temperature from aliquots stored at  $-80^{\circ}\text{C}$ . Samples were diluted 40–240 $\times$  in 0.02  $\mu\text{m}$  filtered PBS to not oversaturate the detector. Before data acquisition, NTA lines were flushed first with 70% ethanol then with 0.02  $\mu\text{m}$  filtered PBS at  $4^{\circ}\text{C}$  to ensure no background signal before sample addition. Typically, 1 mL of sample is loaded into a 1 mL syringe and placed within an automated syringe pump (Harvard Bioscience; MA, USA). Three 30 s video acquisitions were recorded at camera level 12 for each sample. NanoSight NTA 3.1 software was used with detection threshold 2 and default screen gain 10 to track EVs while minimizing any background artifacts. Results for averaged sepsis and control samples are shown in Figure 2f,g. The size distribution graph for each sample is provided in Figure S1.

#### 4.5 | Resistive pulse sensing (RPS)

Resistive pulse sensing (RPS) was performed on nCSI (Spectradyn; CA, USA) using C-400 cartridges (Spectradyn; CA, USA). Buffer solution of 1% Tween 20 and 1% PBS filtered with 0.2  $\mu\text{m}$  non-pyrogenic filter was freshly prepared before each use to lower the surface tension of water. To prime the instrument, a reusable cleaning cartridge was run. Internal standard diluting 200 nm bead (3000 Series Nanosphere Size Standard, Thermo Fisher Scientific; MA, USA) solution was prepared by diluting bead solution 1000 times in buffer solution that was further filtered by a 0.02  $\mu\text{m}$  filter. EV samples were then diluted in the bead solution for a final concentration between  $6 \times 10^9$  and  $2 \times 10^{10}$  particles per mL (minimum of 1:1 dilution). About 3  $\mu\text{L}$  of the EV and bead solution was run on the C-400 cartridge. RPSpass software (version 1.0.2, National Cancer Institute; MD, USA) was then used to analyse the data and remove outliers and bead particles. Results for averaged sepsis and control samples are shown in Figure 2e,g. The size distribution graph for each sample is provided in Figure S1.

#### 4.6 | Single-particle interferometric reflectance imaging sensing (SP-IRIS)

Leprechaun Exosome Human Tetraspanin Kits (Cat. 251–1044, Unchained Labs; CA, USA) were stored in 4°C and chips were warmed to room temperature before use. Chips were pre-scanned to identify any pre-existing adhered particles according to the provided protocol. Isolated EV samples were diluted in 1x incubation solution (provided 10x incubation solution was diluted to 1x concentration with Ultrapure Type I water (18.2 M $\Omega$  cm, PURELAB Chorus, ELGA LabWater, Veolia Water UK Limited; UK) with 0.2% BSA) to achieve between 1000 and 6000 particles per capture spot. For sample incubation, chips were placed in the provided 24-well plate, and 35  $\mu\text{L}$  of diluted EV sample was pipetted onto the centre of the chip. The 24-well plate was then sealed, covered in aluminium foil, and allowed to incubate overnight. After incubation, 300  $\mu\text{L}$  per chip of 1  $\times$  blocking solution and 0.6  $\mu\text{L}$  per chip of anti-CD9, anti-CD63, and anti-CD81 antibodies were prepared. Chips were then washed with the ExoView CW1000 Plate Washer (Unchained Labs; CA, USA) on the CW-TETRA protocol. 250  $\mu\text{L}$  per chip of prepared blocking solution was added when prompted. Chips were then transferred to the chuck and imaged using ExoView RI100 Automated Imager (Unchained Labs; CA, USA). Data was analysed using ExoView Analysis Software (Unchained Labs; CA, USA). Fluorescent cut-offs were chosen to limit the particle count on the MlgG capture spot to be approximately less than 100 events and used for all chips (red channel: 200 a.u., green channel: 250 a.u., blue channel: 450 a.u.). Results for averaged septic and non-septic samples are shown in Figure 2h–j. Tetraspanin expression for each sample is provided in Figure S1.

#### 4.7 | Raman spectral acquisition of EV samples

SEC-isolated EV samples were thawed at room temperature from aliquots stored at  $-80^\circ\text{C}$ . Each sample was homogenized with a Lo-Bind pipette tip, and a 2  $\mu\text{L}$  drop of each sample was placed on 25 mm round quartz coverslips, thickness #1 (0.15–0.18 mm) (SPI Supplies; PA, USA). Note that control patient samples 1880 and 1890 required a second 2  $\mu\text{L}$  droplet to dry to increase the concentration of EVs within the sample for better signal acquisition. Spots were allowed to dry on a hotplate at 45°C for 5 min before measurement. All Raman spectra were acquired using our custom-built inverted Raman scanning confocal microscope with an excitation wavelength of 785 nm. Sample focus was performed manually under a 60  $\times$  1.2 NA water immersion objective on an inverted Olympus IX73 microscope (Olympus Life Science; MA, USA). Spectral capture was performed using an Andor Kymera 328i-C spectrophotometer (Andor Technology Ltd., Oxford Instruments; UK), and both spectral and brightfield images were captured using a Newton DU920P-BR-DD CCD camera (Andor Technology Ltd., Oxford Instruments; UK). Brightfield images were collected using a 0.30 NA lens. Andor Solis version 4.30.30034.0 software (Andor Technology Ltd., Oxford Instruments; UK) was used for acquisition and initial processing. Before each day of measurements, the instrument was calibrated for both wavenumber and intensity, using a Neon reference lamp and NIST traceable SLI-CAL VIS-NIR Tungsten Halogen lamp (StellarNet Inc.; FL, USA), respectively. Five spectra (90-s exposure) were sampled from each patient sample (25 mW laser power at sample, 785 nm excitation wavelength). Spectral data was acquired with a centre wavelength of 850 nm to avoid laser interference, a 2 mm aperture, and a grating of 3 (600 L/mm, blaze 750 nm), allowing for the collection of spectra from 789.42 to 909.88 nm (71.33  $\text{cm}^{-1}$ –1748.39  $\text{cm}^{-1}$ ). Spectra containing cosmic rays were not included.

#### 4.8 | Raman spectral acquisition of LPS and LTA standards

Lipopolysaccharides from *Escherichia coli* O55:B5 irradiated (Product number L6529), Lipopolysaccharides from *Klebsiella pneumoniae*—purified by phenol extraction (Product number L4268), lipopolysaccharides from *Pseudomonas aeruginosa* 10.22 source strain ATCC 27316—purified by phenol extraction (Product number L9143), lipoteichoic acid from *S. aureus* (Product

number L2515), and lipoteichoic acid from *Streptococcus pyogenes* (Product number L3140) were purchased from Sigma Aldrich. Glycoconjugate standards were diluted in Ultrapure Type I water (18.2 M $\Omega$  cm, PURELAB Chorus, ELGA LabWater, Veolia Water UK Limited; UK) based on their respective solubilities, then 2  $\mu$ L of each glycoconjugate standard was dried on 25 mm round quartz coverslips, thickness #1 (0.15–0.18 mm) (SPI Supplies; PA, USA) on a hotplate at 45°C before RS acquisition. LPS from *E. coli* was diluted to 6 mg/mL, LPS from *K. pneumoniae* was diluted to 4 mg/mL, LPS from *P. aeruginosa* was diluted to 6.6 mg/mL, LTA from *S. aureus* was diluted to 2.2 mg/mL, and LTA from *S. pyogenes* was diluted to 5 mg/mL. Each sample underwent Raman spectral acquisition four times. Acquisition parameters and setup were otherwise the same as for the aforementioned patient EV samples. Following spectral processing, an average spectrum for each standard was made by averaging the four acquisitions.

## 4.9 | Raman spectral processing

Spectral processing was performed using an in-house spectral processing GUI script built with MATLAB and carried out using MATLAB r2020b (MathWorks; MA, USA). All spectra were cropped from 700  $\text{cm}^{-1}$  to 1800  $\text{cm}^{-1}$ , background corrected with penalized least-squares, smoothed with a Whitaker Smoothing filter, and intensity normalized using trapezoidal numerical integration so the AUC = 1 for spectral comparisons. Subsequent spectral analysis including principal component analysis, clustering, and linear and quadratic discriminant analysis were also performed utilizing custom-built MATLAB scripts and built-in MATLAB functions/toolboxes.

## 4.10 | Statistical analysis

RPS and NTA average size distribution for sepsis and control samples were determined using GraphPad Prism 10 (Version 10.1.0; GraphPad; San Diego, CA, USA) and Microsoft Excel (Microsoft; Redmond, WA, USA). Values shown for particle total concentration (RPS and NTA) and tetraspanin expression are indicated as the mean  $\pm$  SD. Statistical analysis for particle total concentration (RPS and NTA) was determined using an unpaired *t*-test assuming Gaussian distribution with GraphPad Prism 10 (Version 10.1.0; GraphPad; San Diego, CA, USA). Statistical analysis for tetraspanin expression was determined using an unpaired *t*-test assuming Gaussian distribution with GraphPad Prism 10 (Version 10.1.0; GraphPad; San Diego, CA, USA). All experiments were performed with replicates; NTA and RPS were performed with three replicate runs per sample, multiple CryoEM grids were prepared for representative samples for each group, and each Raman measurement was performed five times for each patient sample and four times for the glycoconjugate standards. Statistical significance was considered when  $p < 0.05$ .

## AUTHOR CONTRIBUTIONS

Hannah J. O'Toole: Conceptualization (lead); Data curation (lead); Formal analysis (lead); Investigation (lead); Methodology (lead); Visualization (lead); Writing—original draft (lead). Randy P. Carney: Conceptualization (lead); data curation (supporting); formal analysis (supporting); funding acquisition (lead); project administration (lead); software (lead); supervision (lead); visualization (supporting); writing—original draft (supporting); writing—review and editing (supporting). Neona M. Lowe: Data curation (supporting); formal analysis (supporting); writing—review and editing (supporting). Vishalakshi Arun: Investigation (supporting). Anna V. Kolesov: Data curation (supporting); formal analysis (supporting); writing—review and editing (supporting). Tina L. Palmieri: Project administration (supporting); resources (supporting); writing—review and editing (supporting). Nam K. Tran: Project administration (supporting); resources (supporting); writing—review and editing (supporting).

## ACKNOWLEDGEMENTS

This work was financially supported by the National Institutes of Health (NIH) by Award Number R01 CA241666. H.J.O. acknowledges T32 GM136597-03. N.M.L. acknowledges T32 HL007013. The funders had no roles in the study design, data collection, data analysis, decision to publish, or preparation of the manuscript. The content of this work is solely the product of the authors and does not necessarily represent the views of the funding parties. Components of figures in this work were created using BioRender.com. Specimens were provided by the UC Davis Pathology Biorepository. Cryo-electron microscopy was performed at the UC Davis BioEM Facility in Briggs Hall. The UC Davis BioEM Facility is supported by user fees, the Department of Molecular and Cellular Biology, the College of Biosciences, the Office of Research and the Provost's Office. The Technical Director, Dr. Fei Guo, is supported by discretionary funds provided by MCB. The K3 and DED detectors were purchased from funding support provided by the Department of Molecular and Cellular Biology, College of Biological Sciences, and grant support provided by R00-GM080249 (J. Al-Bassam).

## CONFLICT OF INTEREST STATEMENT

The authors declare no conflicts of interest.

## DATA AVAILABILITY STATEMENT

All raw datasets generated and analysed during the current study are freely available on a Zenodo repository with the identifier <https://doi.org/10.5281/zenodo.11194408>.

## ORCID

Hannah J. O'Toole  <https://orcid.org/0000-0002-1843-9332>

Neona M. Lowe  <https://orcid.org/0000-0002-7426-0273>

Anna V. Kolesov  <https://orcid.org/0009-0006-3870-7644>

Tina L. Palmieri  <https://orcid.org/0000-0001-6340-1715>

Nam K. Tran  <https://orcid.org/0000-0003-1565-0025>

Randy P. Carney  <https://orcid.org/0000-0001-8193-1664>

## REFERENCES

- Avni, T., Levcovich, A., Ad-El, D. D., Leibovici, L., & Paul, M. (2010). Prophylactic antibiotics for burns patients: Systematic review and meta-analysis. *BMJ*, *340*, c241.
- Bachurski, D., Schuldner, M., Nguyen, P. H., Malz, A., Reiners, K. S., Grenzi, P. C., Babatz, F., Schauss, A. C., Hansen, H. P., Hallek, M., & Pogge von Strandmann, E. (2019). Extracellular vesicle measurements with nanoparticle tracking analysis—An accuracy and repeatability comparison between NanoSight NS300 and ZetaView. *Journal of Extracellular Vesicles*, *8*(1), 1596016.
- Bishop, D. G., & Work, E. (1965). An extracellular glycolipid produced by *Escherichia coli* grown under lysine-limiting conditions. *Biochemical Journal*, *96*, 567–576.
- Boehm, D., & Menke, H. (2021). Sepsis in burns—Lessons learnt from developments in the management of septic shock. *Medicina*, *58*, 26.
- Bouza, E., Onori, R., Semiglia-Chong, M. A., Álvarez-Uría, A., Alcalá, L., & Burillo, A. (2020). Fast track SSTI management program based on a rapid molecular test (GeneXpert® MRSA/SA SSTI) and antimicrobial stewardship. *Journal of Microbiology, Immunology, and Infection*, *53*, 328–335.
- Burn Triage and Treatment—Thermal Injuries. Chemical Hazards Emergency Medical Management (CHEMM), U.S. Department of Health & Human Services. <https://chemm.hhs.gov/burns.html>. (accessed 19 July 2024)
- Cardoso, L. T., Grion, C. M., Matsuo, T., Anami, E. H., Kauss, I. A., Seko, L., & Bonametti, A. M. (2011). Impact of delayed admission to intensive care units on mortality of critically ill patients: A cohort study. *Critical Care (London, England)*, *15*(1), R28.
- Chakraborty, R. K., & Burns, B. (2023). Systemic inflammatory response syndrome. *StatPearls*, StatPearls Publishing.
- Chaudhry, H., Zhou, J., Zhong, Y., Ali, M. M., McGuire, F., Nagarkatti, P. S., & Nagarkatti, M. (2013). Role of cytokines as a double-edged sword in sepsis. *In Vivo (Athens, Greece)*, *27*(6), 669–684.
- Chela, H. K., Vasudevan, A., Rojas-Moreno, C., & Naqvi, S. H. (2019). Approach to positive blood cultures in the hospitalized patient: A review. *Missouri Medicine*, *116*, 313–317.
- Chen, Z., Turxun, N., & Ning, F. (2021). Meta-analysis of the diagnostic value of procalcitonin in adult burn sepsis. *Advances in Clinical and Experimental Medicine*, *30*, 455–463.
- Church, D., Elsayed, S., Reid, O., Winston, B., & Lindsay, R. (2006). Burn wound infections. *Clinical Microbiology Reviews*, *19*, 403–434.
- Ciferri, M. C., Quarto, R., & Tasso, R. (2021). Extracellular vesicles as biomarkers and therapeutic tools: From pre-clinical to clinical applications. *Biology (Basel)*, *10*, 359.
- Couch, Y., Buzàs, E. I., Di Vizio, D., Gho, Y. S., Harrison, P., Hill, A. F., Lötvall, J., Raposo, G., Stahl, P. D., Théry, C., Witwer, K. W., & Carter, D. R. F. (2021). A brief history of nearly everything—The rise and rise of extracellular vesicles. *Journal of Extracellular Vesicles*, *10*(14), e12144.
- Dahal, M., & Schwan, W. R. (2018). Management of methicillin-resistant *Staphylococcus aureus* mediated ventilator-associated pneumonia. *Current Trends in Microbiology*, *12*, 95–107.
- Dal Ponte, S. T., Alegretti, A. P., Pilger, D. A., Rezende, G. P., Andrioli, G., Ludwig, H. C., Diogo, L., Goldani, L. Z., Loreto, M., Machado, P. S., & Seligman, R. (2018). Diagnostic accuracy of CD64 for sepsis in emergency department. *Journal of Global Infectious Diseases*, *10*(2), 42–46.
- Deathage, B. L., & Cookson, B. T. (2012). Membrane vesicle release in bacteria, eukaryotes, and archaea: A conserved yet underappreciated aspect of microbial life. *Infection and Immunity*, *80*, 1948–1957.
- Dierig, A., Berger, C., Agyeman, P. K. A., Bernhard-Stirneemann, S., Giannoni, E., Stocker, M., Posfay-Barbe, K. M., Niederer-Loher, A., Kahlert, C. R., Donas, A., Hasters, P., Rely, C., Riedel, T., Aebi, C., Schlapbach, L. J., Heininger, U., & Swiss Pediatric Sepsis Study. (2018). Time-to-positivity of blood cultures in children with sepsis. *Frontiers in Pediatrics*, *6*, 222.
- Forward, D. W., & Garon, C. F. (1990). DNA is packaged within membrane-derived vesicles of gram-negative but not gram-positive bacteria. *Applied and Environmental Microbiology*, *56*, 1960–1962.
- Egea-Guerrero, J. J., & Rodríguez-Rodríguez, A. (2016). Sepsis biomarkers in severe burn patients: Cut-off point or time profile? *Medicina Intensiva*, *40*, 595–596.
- Eilers, P. H. C. (2003). A perfect smoother. *Analytical Chemistry*, *75*, 3631–3636.
- Farhana, A., & Khan, Y. S. (2024). Biochemistry, lipopolysaccharide. *StatPearls*, StatPearls Publishing.
- Fournier, B., & Philpott, D. J. (2005). Recognition of *Staphylococcus aureus* by the innate immune system. *Clinical Microbiology Reviews*, *18*, 521–540.
- Fu, S., Zhang, Y., Li, Y., Luo, L., Zhao, Y., & Yao, Y. (2020). Extracellular vesicles in cardiovascular diseases. *Cell Death Discovery*, *6*, 68.
- Gabarin, R. S., Li, M., Zimmel, P. A., Marshall, J. C., Li, Y., & Zhang, H. (2021). Intracellular and extracellular lipopolysaccharide signaling in sepsis: Avenues for novel therapeutic strategies. *Journal of Innate Immunity*, *13*(6), 323–332.
- Gill, C. M., Dolan, L., Piggott, L. M., & McLaughlin, A. M. (2022). New developments in tuberculosis diagnosis and treatment. *Breathe*, *18*, 210149.
- Gille, J., Jovicic, J., Kremer, T., & Sablotzki, A. (2021). The predictive role of interleukin 6 in burn patients with positive blood cultures. *International Journal of Burns and Trauma*, *11*(2), 123–130.
- Gomez, R., Murray, C. K., Hospenthal, D. R., Cancio, L. C., Renz, E. M., Holcomb, J. B., Wade, C. E., & Wolf, S. E. (2009). Causes of mortality by autopsy findings of combat casualties and civilian patients admitted to a burn unit. *Journal of the American College of Surgeons*, *208*(3), 348–354.
- Green, L. R., Monk, P. N., Partridge, L. J., Morris, P., Gorringer, A. R., & Read, R. C. (2011). Cooperative role for tetraspanins in adhesin-mediated attachment of bacterial species to human epithelial cells. *Infection and Immunity*, *79*(6), 2241–2249.
- Gregoriano, C., Heilmann, E., Molitor, A., & Schuetz, P. (2020). Role of procalcitonin use in the management of sepsis. *Journal of Thoracic Disease*, *12*, S5–S15.

- Hauptmann, A., Hoelzl, G., Mueller, M., Bechtold-Peters, K., & Loerting, T. (2023). Raman marker bands for secondary structure changes of frozen therapeutic monoclonal antibody formulations during thawing. *Journal of Pharmaceutical Sciences*, *112*, 51–60.
- Hemler, M. E. (2005). Tetraspanin functions and associated microdomains. *Nature Reviews Molecular Cell Biology*, *6*, 801–811.
- Hill, A. F. (2019). Extracellular vesicles and neurodegenerative diseases. *Journal of Neuroscience*, *39*, 9269–9273.
- Hill, D. M., Percy, M. D., Velamuri, S. R., Lanfranco, J., Romero Legro, I., Sinclair, S. E., & Hickerson, W. L. (2018). Predictors for identifying burn sepsis and performance vs existing criteria. *Journal of Burn Care & Research: Official Publication of the American Burn Association*, *39*(6), 982–988.
- Hobro, A. J., Rouhi, M., Blanch, E. W., & Conn, G. L. (2007). Raman and Raman optical activity (ROA) analysis of RNA structural motifs in domain I of the EMCV IRES. *Nucleic Acids Research*, *35*, 1169–1177.
- Hogan, B. K., Wolf, S. E., Hospenthal, D. R., D'Avignon, L. C., Chung, K. K., Yun, H. C., Mann, E. A., & Murray, C. K. (2012). Correlation of American Burn Association sepsis criteria with the presence of bacteremia in burned patients admitted to the intensive care unit. *Journal of Burn Care & Research: Official Publication of the American Burn Association*, *33*(3), 371–378.
- Horgan, C. C., Nagelkerke, A., Whittaker, T. E., Nele, V., Massi, L., Kauscher, U., Penders, J., Bergholt, M. S., Hood, S. R., & Stevens, M. M. (2020). Molecular imaging of extracellular vesicles in vitro via Raman metabolic labelling. *Journal of Materials Chemistry B*, *8*(20), 4447–4459.
- Huang, X., Yuan, T., Tschannen, M., Sun, Z., Jacob, H., Du, M., Liang, M., Dittmar, R. L., Liu, Y., Liang, M., Kohli, M., Thibodeau, S. N., Boardman, L., & Wang, L. (2013). Characterization of human plasma-derived exosomal RNAs by deep sequencing. *BMC Genomics*, *14*, 319.
- Jenkins, C. L., & Bean, H. D. (2023). Current limitations of staph infection diagnostics, and the role for VOCs in achieving culture-independent detection. *Pathogens*, *12*, 181.
- Jeong, H., Han, C., Cho, S., Gianchandani, Y., & Park, J. (2018). Analysis of extracellular vesicles using coffee ring. *ACS Applied Materials & Interfaces*, *10*, 22877–22882.
- Jeong, H., Shin, H., Yi, J., Park, Y., Lee, J., Gianchandani, Y., & Park, J. (2019). Size-based analysis of extracellular vesicles using sequential transfer of an evaporating droplet. *Lab on a Chip*, *19*(19), 3326–3336.
- Jnana, A., Shiek, S. S., Satyamoorthy, K., & Murali, T. S. (2023). Extracellular vesicles in bacterial and fungal diseases—Pathogenesis to diagnostic biomarkers. *Virulence*, *14*, 2180934.
- Karam, J., Méresse, S., Kremer, L., & Daher, W. (2020). The roles of tetraspanins in bacterial infections. *Cellular Microbiology*, *22*, e13260.
- Kazemzadeh, M., Hisey, C., Singorenko, P. D., Swift, S., Zargar, K., Xu, P., & Broderick, N. (2022). Label-free classification of bacterial extracellular vesicles by combining nanoplasmonic sensors with machine learning. *IEEE Sensors Journal*, *22*, 1128–1137.
- Koster, H. J., Rojalín, T., Powell, A., Pham, D., Mizenko, R. R., Birkeland, A. C., & Carney, R. P. (2021). Surface enhanced Raman scattering of extracellular vesicles for cancer diagnostics despite isolation dependent lipoprotein contamination. *Nanoscale*, *13*(35), 14760–14776.
- Lavrentieva, A., Kontakiotis, T., Lazaridis, L., Tsotsolis, N., Koumis, J., Kyriazis, G., & Bitzani, M. (2007). Inflammatory markers in patients with severe burn injury. What is the best indicator of sepsis? *Burns: Journal of the International Society for Burn Injuries*, *33*, 189–194.
- Lee, S. M., & An, W. S. (2016). New clinical criteria for septic shock: Serum lactate level as new emerging vital sign. *Journal of Thoracic Disease*, *8*, 1388–1390.
- Lekkou, A., Karakantza, M., Mouzaki, A., Kalfarentzos, F., & Gogos, C. A. (2004). Cytokine production and monocyte HLA-DR expression as predictors of outcome for patients with community-acquired severe infections. *Clinical and Diagnostic Laboratory Immunology*, *11*, 161–167.
- Li, A. T., Moussa, A., Gus, E., Paul, E., Yii, E., Romero, L., Lin, Z. C., Padiglione, A., Lo, C. H., Cleland, H., & Cheng, A. C. (2022). Biomarkers for the early diagnosis of sepsis in burns: Systematic review and meta-analysis. *Annals of Surgery*, *275*(4), 654–662.
- Mangini, M., Verde, A., Boraschi, D., Puentes, V. F., Italiani, P., & De Luca, A. C. (2021). Interaction of nanoparticles with endotoxin importance in nanosafety testing and exploitation for endotoxin binding. *Nanotoxicology*, *15*(4), 558–576.
- Mann-Salinas, E. A., Baun, M. M., Meininger, J. C., Murray, C. K., Aden, J. K., Wolf, S. E., & Wade, C. E. (2013). Novel predictors of sepsis outperform the American Burn Association sepsis criteria in the burn intensive care unit patient. *Journal of Burn Care & Research: Official Publication of the American Burn Association*, *34*(1), 31–43.
- Martin, G. S., Mannino, D. M., Eaton, S., & Moss, M. (2003). The epidemiology of sepsis in the United States from 1979 through 2000. *New England Journal of Medicine*, *348*, 1546–1554.
- Naruskaitė, D., Vydmantaitė, G., Rusteikaitė, J., Sampath, R., Rudaitytė, A., Stašytė, G., Aparicio Calvente, M. I., & Jekabsone, A. (2021). Extracellular vesicles in skin wound healing. *Pharmaceuticals (Basel, Switzerland)*, *14*(8), 811.
- Neugebauer, U., Trenkmann, S., Bocklitz, T., Schmerler, D., Kiehntopf, M., & Popp, J. (2014). Fast differentiation of SIRS and sepsis from blood plasma of ICU patients using Raman spectroscopy. *Journal of Biophotonics*, *7*, 232–240.
- Neuhaus, F. C., & Baddiley, J. (2003). A continuum of anionic charge: Structures and functions of D-alanyl-teichoic acids in gram-positive bacteria. *Microbiology and Molecular Biology Reviews*, *67*, 686–723.
- Nottingham, I. (2007). 12 - Characterisation using Raman micro-spectroscopy. In Boccaccini, A. R. & Gough, J. E. (Eds.). *Tissue engineering using ceramics and polymers* (pp. 248–266). Woodhead Publishing.
- Nottingham, I., Verrier, S., Haque, S., Polak, J. M., & Hench, L. L. (2003). Spectroscopic study of human lung epithelial cells (A549) in culture: Living cells versus dead cells. *Biopolymers*, *72*, 230–240.
- Nyquist, R. A. (1971). Raman group frequency correlations: Phthalate esters. *Applied Spectroscopy*, *26*, 81–85.
- Osorio-Román, I. O., Aroca, R. F., Astudillo, J., Matsuhiro, B., Vásquez, C., & Pérez, J. M. (2010). Characterization of bacteria using its O-antigen with surface-enhanced Raman scattering. *The Analyst*, *135*, 1997–2001.
- Pappas, D., Smith, B. W., & Winefordner, J. D. (2000). Raman spectroscopy in bioanalysis. *Talanta*, *51*, 131–144.
- Pileri, D., Accardo Palombo, A., D'Amelio, L., D'Arpa, N., Amato, G., Masellis, A., Cataldo, V., Mogavero, R., Napoli, B., Lombardo, C., & Conte, C. (2008). Concentrations of cytokines IL-6 and IL-10 in plasma of burn patients: Their relationship to sepsis and outcome. *Annals of Burns and Fire Disasters*, *21*(4), 182–185.
- Pope, J. L., Tomkovich, S., Yang, Y., & Jobin, C. (2017). Microbiota as a mediator of cancer progression and therapy. *Translational Research*, *179*, 139–154.
- Qin, Y. F., Lu, X. Y., Shi, Z., Huang, Q. S., Wang, X., Ren, B., & Cui, L. (2022). Deep learning-enabled Raman spectroscopic identification of pathogen-derived extracellular vesicles and the biogenesis process. *Analytical Chemistry*, *94*(36), 12416–12426.
- qSOFA. quick sepsis related organ failure assessment. <https://qsofa.org/>
- Ramachandran, G. (2014). Gram-positive and gram-negative bacterial toxins in sepsis: A brief review. *Virulence*, *5*, 213.
- Raman, C. V. (1929). Part II.—The Raman effect. Investigation of molecular structure by light scattering. *Transactions of the Faraday Society*, *25*, 781–792.
- Randolph, T. W. (2006). Scale-based normalization of spectral data. *Cancer Biomark*, *2*, 135–144.
- Rudd, K. E., Johnson, S. C., Agesa, K. M., Shackelford, K. A., Tsoi, D., Kievlan, D. R., Colombara, D. V., Ikuta, K. S., Kissoon, N., Finfer, S., Fleischmann-Struzek, C., Machado, F. R., Reinhart, K. K., Rowan, K., Seymour, C. W., Watson, R. S., West, T. E., Marinho, F., Hay, S. I., ... Naghavi, M. (2020). Global,



- regional, and national sepsis incidence and mortality, 1990–2017: Analysis for the Global Burden of Disease Study. *Lancet (London, England)*, 395, 200–211.
- Schneewind, O., & Missiakas, D. (2014). Lipoteichoic acids, phosphate-containing polymers in the envelope of gram-positive bacteria. *Journal of Bacteriology*, 196, 1133–1142.
- Shahsavarinia, K., Moharramzadeh, P., Arvanagi, R. J., & Mahmoodpoor, A. (2020). qSOFA score for prediction of sepsis outcome in emergency department. *Pakistan Journal of Medicinal Sciences*, 36, 668–672.
- Shankar-Hari, M., Phillips, G. S., Levy, M. L., Seymour, C. W., Liu, V. X., Deutschman, C. S., Angus, D. C., Rubenfeld, G. D., Singer, M., & Sepsis Definitions Task Force. (2016). Developing a new definition and assessing new clinical criteria for septic shock: For the third international consensus definitions for sepsis and septic shock (Sepsis-3). *JAMA*, 315, 775–787.
- Singer, M., Deutschman, C. S., Seymour, C. W., Shankar-Hari, M., Annane, D., Bauer, M., Bellomo, R., Bernard, G. R., Chiche, J. D., Cooper-Smith, C. M., Hotchkiss, R. S., Levy, M. M., Marshall, J. C., Martin, G. S., Opal, S. M., Rubenfeld, G. D., van der Poll, T., Vincent, J. L., & Angus, D. C. (2016). The third international consensus definitions for sepsis and septic shock (Sepsis-3). *JAMA*, 315, 801–810.
- Stähle, L., & Wold, S. (1987). Partial least squares analysis with cross-validation for the two-class problem: A Monte Carlo study. *Journal of Chemometrics*, 1, 185–196.
- Théry, C., Witwer, K. W., Aikawa, E., Alcaraz, M. J., Anderson, J. D., Andriantsitohaina, R., Antoniou, A., Arab, T., Archer, F., Atkin-Smith, G. K., Ayre, D. C., Bach, J. M., Bachurski, D., Baharvand, H., Balaj, L., Baldacchino, S., Bauer, N. N., Baxter, A. A., Bebawy, M., ... Zuba-Surma, E. K. (2018). Minimal information for studies of extracellular vesicles 2018 (MISEV2018): A position statement of the International Society for Extracellular Vesicles and update of the MISEV2014 guidelines. *Journal of Extracellular Vesicles*, 7, 1535750.
- Tian, C., Wang, K., Zhao, M., Cong, S., Di, X., & Li, R. (2022). Extracellular vesicles participate in the pathogenesis of sepsis. *Frontiers in Cellular and Infection Microbiology*, 12, 1018692.
- Tian, C. M., Yang, M. F., Xu, H. M., Zhu, M. Z., Zhang, Y., Yao, J., Wang, L. S., Liang, Y. J., & Li, D. F. (2023). Emerging role of bacterial outer membrane vesicle in gastrointestinal tract. *Gut Pathogens*, 15, 20.
- Tuberculosis (TB). <https://www.who.int/news-room/fact-sheets/detail/tuberculosis>
- van der Vaart, T. W., Prins, J. M., Soetekouw, R., van Twillert, G., Veenstra, J., Herpers, B. L., Rozemeijer, W., Jansen, R. R., Bonten, M. J. M., & van der Meer, J. T. M. (2022). All-cause and infection-related mortality in *Staphylococcus aureus* bacteremia, a multicenter prospective Cohort study. *Open Forum Infectious Diseases*, 9, ofac653.
- EV-TRACK Consortium. Van Deun, J., Mestdagh, P., Agostinis, P., Akay, Ö., Anand, S., Anckaert, J., Martinez, Z. A., Baetens, T., Beghein, E., Bertier, L., Berx, G., Boere, J., Boukouris, S., Bremer, M., Buschmann, D., Byrd, J. B., Casert, C., Cheng, L., ... Hendrix, A. (2017). EV-TRACK: Transparent reporting and centralizing knowledge in extracellular vesicle research. *Nature Methods*, 14(3), 228–232.
- von Aulock, S., Morath, S., Hareng, L., Knapp, S., van Kessel, K. P., van Strijp, J. A., & Hartung, T. (2003). Lipoteichoic acid from *Staphylococcus aureus* is a potent stimulus for neutrophil recruitment. *Immunobiology*, 208(4), 413–422.
- Wang, Y., Xu, J., Kong, L., Li, B., Li, H., Huang, W. E., & Zheng, C. (2020). Raman-activated sorting of antibiotic-resistant bacteria in human gut microbiota. *Environmental Microbiology*, 22, 2613–2624.
- Welsh, J. A., Goberdhan, D. C. I., O'Driscoll, L., Buzas, E. I., Blenkiron, C., Bussolati, B., Cai, H., Di Vizio, D., Driedonks, T. A. P., Erdbrügger, U., Falcon-Perez, J. M., Fu, Q. L., Hill, A. F., Lenassi, M., Lim, S. K., Mahoney, M. G., Mahanty, S., Möller, A., ... Witwer, K. W. (2024). Minimal information for studies of extracellular vesicles (MISEV2023): From basic to advanced approaches. *Journal of Extracellular Vesicles*, 13(2), e12404.
- Whittaker, E. T. (1922). On a new method of graduation. *Proceedings of the Edinburgh Mathematical Society*, 41, 63–75.
- Wu, X., Zhao, Y., & Zughaier, S. M. (2021). Highly sensitive detection and differentiation of endotoxins derived from bacterial pathogens by surface-enhanced Raman scattering. *Biosensors*, 11, 234.
- Xu, R., Rai, A., Chen, M., Suwakulsiri, W., Greening, D. W., & Simpson, R. J. (2018). Extracellular vesicles in cancer—Implications for future improvements in cancer care. *Nature Reviews. Clinical Oncology*, 15(10), 617–638.
- Yan, J., Hill, W. F., Rehov, S., Pinto, R., Shahrokhi, S., & Jeschke, M. G. (2018). Sepsis criteria versus clinical diagnosis of sepsis in burn patients: A validation of current sepsis scores. *Surgery*, 164(6), 1241–1245.
- Yang, Y., Xu, B., Haverstick, J., Ibtehaz, N., Muszyński, A., Chen, X., Chowdhury, M. E. H., Zughaier, S. M., & Zhao, Y. (2022). Differentiation and classification of bacterial endotoxins based on surface enhanced Raman scattering and advanced machine learning. *Nanoscale*, 14(24), 8806–8817.
- Zaborowski, M. P., Balaj, L., Breakefield, X. O., & Lai, C. P. (2015). Extracellular vesicles: Composition, biological relevance, and methods of study. *Bioscience*, 65, 783–797.
- Zhang, Z.-M., Chen, S., & Liang, Y.-Z. (2010). Baseline correction using adaptive iteratively reweighted penalized least squares. *Analyst*, 135, 1138–1146.

## SUPPORTING INFORMATION

Additional supporting information can be found online in the Supporting Information section at the end of this article.

**How to cite this article:** O'Toole, H. J., Lowe, N. M., Arun, V., Kolesov, A. V., Palmieri, T. L., Tran, N. K., & Carney, R. P. (2024). Plasma-derived extracellular vesicles (EVs) as biomarkers of sepsis in burn patients via label-free Raman spectroscopy. *Journal of Extracellular Vesicles*, 13, e12506. <https://doi.org/10.1002/jev2.12506>